ChemPubSoc Europe

DOI: 10.1002/batt.201800022

BATTERIES & SUPERCAPS
Articles

Improving the Performance of Batteries by Using Multi-Pyrene PTMA Structures

Noémie Hergué,*[a] Bruno Ernould,[b] Andrea Minoia,[c] Roberto Lazzaroni,[c] Jean-François Gohy,[b] Philippe Dubois,[a] and Olivier Coulembier*[a]

Well-defined pyrene-based poly(2,2,6,6-tetramethylpiperidinyloxy-4-yl methacrylate) (PTMA) (co)polymers have been synthesized and combined with multi-wall carbon nanotubes (CNTs) as electrode material for organic radical batteries. The influence of the number of pyrene pendent groups on the electrochemical response of the nanocomposite materials has been assessed, focusing on the capacity retention upon charge/discharge cycling and on the cycling rate. In parallel, the interactions between the polymethacrylate chains and the CNT surface have been investigated with molecular modeling techniques, to shed light on the nature and stability of the functionalized PTMA/CNT interface.

1. Introduction

Lithium-ion batteries (LiBs) are currently the prevalent technology used to store energy.[1] Their high energy density makes them a choice technology for portable applications. A complementary technology lies in supercapacitors, providing high power but suffering from a poor energy density compared to Li-ion batteries.[2] A technology able to combine the advantage of LiBs and capacitors is emerging with the development of organic radical batteries (ORBs).[3,4] Among the different organic functions that can be used to store electrical energy via reversible redox reactions, stable organic radicals have shown great potential as active materials for the fabrication of cathodes because of their high stability and the reversibility of their redox reactions, allowing good cycling properties. Various redox-active radical materials have been investigated so far, such as galvinoxyl,[5,6] diphenylpicrylhydrazyl (DPPH)[5,6] and nitroxide radical derivatives.[7] In particular, the well-known (2,2,6,6-tetramethylpiperidin-1-yl)oxyl group, TEMPO, has received much interest but needs to be immobilized into a crosslinked polymer network because of its solubility in common electrolytes for Li-ion batteries (especially in carbonates). For this purpose, the TEMPO group is usually introduced as a pendent moiety on a methacrylate backbone to lead to the poly(2,2,6,6-tetramethylpiperidinyloxy-4-yl methacrylate) (PTMA) redox-active polymer. PTMA shows two reversible redox processes: oxidation of the nitroxide radical into the oxoammonium cation around 3.6 V (vs. Li/Li^+) and a reduction of the nitroxide radical into the aminoxyl anion around 2.6 V (vs. Li/Li^+). PTMA shows a theoretical capacity of 111 $mAh\,g^{-1}$, a good cycling stability attributed to high radical stability, fast charging and a high-power capability.[5,8] Nevertheless, PTMA is an insulating polymer and has to be blended with a good conductor to target battery applications. To date, various conductive charges including graphene sheets, graphene oxide sheets and carbon nanotubes (CNTs) have been associated to PTMA.[9,10] Another drawback of PTMA is its solubility in electrolytes.[3] To overcome this issue different approaches have been followed: Zhang et al. showed that the PTMA molecular weight has a major effect on the polymer solubility and thus, on its electrochemical properties.[11] In addition, both, capacity and rate performance are much better with PTMA of high molar masses. Another way to decrease the solubility of the active material is to use cross-linked PTMA, creating a polymer network[12–14] or to graft PTMA on the conductive material.[12,15–17] Non-covalent interactions between PTMA and the conductive material have also been considered with imidazolium[18] (cation-π interaction) and pyrene[19] (π-π stacking) as anchoring points to immobilize PTMA onto nanostructured carbon derivatives. Zhang et al. recently reported a non-covalent interaction between a pyrene-functionalized PTMA and reduced graphene oxide (rGO).[19] In that study, a two-electron redox process promoted by the rGO led to high capacities. To the best of our knowledge that highly relevant work represents the first example of a pyrene-based PTMA used in batteries so far.

Since the PTMA/rGO composites developed by Zhang present a decrease in capacity (from 1 to 10–20C) when submitted to variable rates, here we have decided to inves-

[a] Dr. N. Hergué, Prof. P. Dubois, Prof. O. Coulembier
Laboratory of Polymeric and Composite Materials (LPCM)
Center of Innovation and Research in Materials and Polymers (CIRMAP)
University of Mons-UMONS
20 Place du Parc, B-7000 Mons, Belgium
E-mail: noemie.hergue@umons.ac.be
olivier.coulembier@umons.ac.be
[b] B. Ernould, Prof. J.-F. Gohy
Institute of Condensed Matter and Nanosciences (IMCN)
Bio- and Soft Matter (BSMA)
Université catholique de Louvain
Place L. Pasteur 1, B-1348, Louvain-la-Neuve, Belgium
[c] Dr. A. Minoia, Prof. R. Lazzaroni
Laboratory for Chemistry of Novel Materials
Center of Innovation and Research in Materials and Polymers (CIRMAP)
University of Mons-UMONS
20 Place du Parc, B-7000 Mons, Belgium
Supporting Information and the ORCID identification number(s) for the author(s) of this article can be found under:
https://doi.org/10.1002/batt.201800022

tigate the importance of the number of pyrene units anchored along the PTMA chain to improve the performance of the corresponding PTMA/CNT nanocomposites. In this work, two pyrene-based PTMA structures have been studied and used with multi-wall CNTs (MWCNTs): the first one is a PTMA polymer bearing a single pyrene end-group; it was intentionally designed to confer a low steric hindrance and less conformational constraints to the homopolymer, when the pyrene interacts with the carbon surface. For the second system, pyrene units have been incorporated along the PTMA chain, by copolymerization of a pyrene-substituted methacrylate with the TEMPO-substituted methacrylate. The influence of the macromolecular architecture on the electrochemical response has been assessed, focusing on the capacity retention upon cycling and on the cycling rate. To shed light on the nature and stability of the functionalized PTMA/CNT interface, the interactions between the (co)polymer chains and the carbon surface have been investigated with molecular modeling techniques in parallel.

The main drawback encountered when organic electrodes are prepared from a simple physical mixing of PTMA and CNTs remains on the partial migration of PTMA out of the electrode during the battery operation, due to its solubility in the battery electrolyte. Cross-linking of PTMA has been proposed as a solution to that issue, but the process raises other challenges, such as: (i) problems of processing due to the insolubility of cross-linked PTMA in the solvents used during electrode fabrication, (ii) impossibility to obtain close contact between conductive carbon-based materials, e.g., CNTs, and crosslinked PTMA particles, (iii) non-homogeneous crosslinking of PTMA, leading to the release of non-crosslinked chains. One way to circumvent those drawbacks would be to directly attach PTMA chains on conductive carbon-based materials. In this respect, Ernould et al. grafted PTMA to CNTs via "grafting from"[20] and "grafting onto" techniques.[21] The PTMA could thus be immobilized on the electrode, leading to electrochemical cells with higher capacity and stability. The "grafting onto" approach allows a better control of the material characterization than the "grafting from" technique. However, both grafting methods involve covalent chemical modifications of the CNTs disrupting the conductive network of sp^2 carbon atoms along the nanotube and reducing their inherent conductivity.[22,23]

Taking advantage of non-covalent/supramolecular interactions would allow a close contact between CNTs and PTMA chains without modifying the CNT network and therefore their conductivity. In this study, two kinds of (co)polymer structures were considered to reach such a goal: a PTMA end-functionalized at one end by a single pyrene molecule, i.e., able to interact with the CNT surface via π-π bonding, and a PTMA bearing multiple pyrene molecules as side groups and one pyrene as chain-end. A single terminal pyrene unit is expected to promote the immobilization of PTMA chains on the CNT by their extremity while a multi-pyrene structure would favor interaction of the whole PTMA chain with the CNT.

2. Results and Discussion

2.1. Synthesis of PTMA-Based (Co)Polymers

The controlled synthesis of PTMA-based (co)polymers was achieved via atom transfer radical (co)polymerization (ATRP). Since the dangling nitroxide groups of the PTMA can be readily obtained by oxidation of the corresponding secondary amine, 2,2,6,6-tetramethyl-4-piperidyl methacrylate (TMPM) has been used as comonomer in the process.

The typical synthesis via ATRP of PTMA-based (co)polymers is depicted on Figure 1.

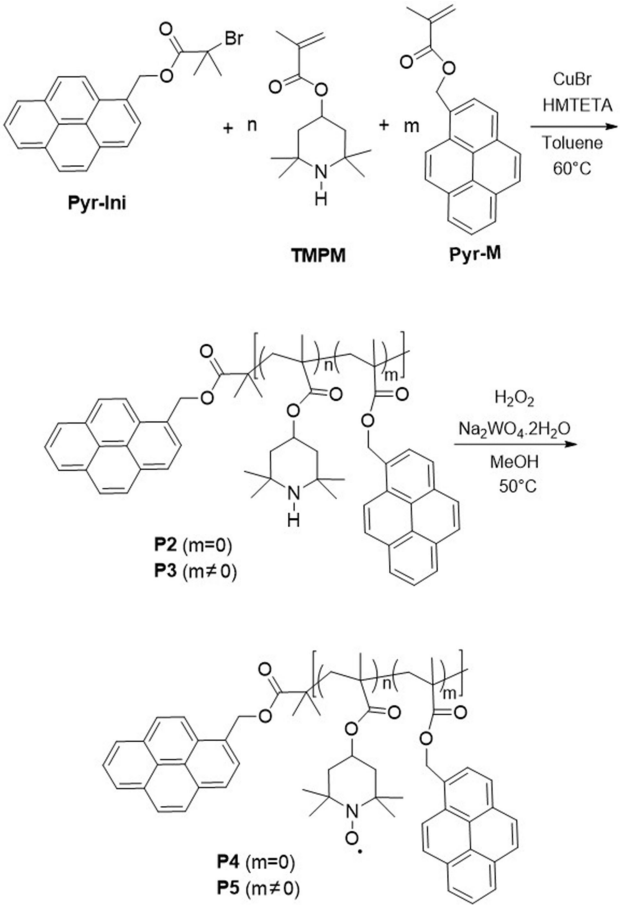

Figure 1. Synthetic routes toward the formation of PTMA-based (co) polymers via (co)polymerization of the TMPM precursor monomer by ATRP followed by oxidation of the amine groups into nitroxides.

The synthesis of pyrene-terminated polymers was performed by homopolymerization of the TMPM starting from a pyrene methyl-α-bromoisobutyrate (Pyr-Ini) initiator (Figure S1). The use of Pyr-Ini allows an efficient functionalization of the polymer as well as an easy determination of the polymerization degree (DP) by ^{1}H-NMR, due to the distinct peaks of the pyrene unit in the aromatic region.

Prior to any copolymerization, the homopolymerization of TMPM was first performed to assess the possibility to control the ATRP process of such a monomer. To that end, TMPM was

polymerized by using a CuBr/HMTETA catalytic complex ($[CuBr]_0/[HMTETA]_0 = 0.5$) in toluene ($[TMPM]_0 = 3.2$ mol/L) at 60 °C from a freshly prepared pyrene methyl-α-bromoisobutyrate initiator.[24] The reaction times were adapted according to the targeted DP. As presented in Table 1, poly(2,2,6,6-tetramethylpiperidine methacrylate) (PTMPM) homopolymers (entries 2–3) of variable molar masses have been obtained presenting narrow dispersity indices ($M_w/M_n = Đ < 1.3$). In order to highlight the importance of the pyrene moiety on the final material properties, a non-functionalized PTMPM homopolymer has been prepared by using ethyl bromoisobutyryl bromide as initiator (Entry 1, Table 1).

Table 1. Molecular characterizations of the PTMPM homopolymers.

Entry	Code	R-Ini	n[a]	$Mn_{(NMR)}$[a] [g mol^{-1}]	$Mn_{(SEC)}$[b] [g mol^{-1}]	Đ[b]
1	P1	Ethyl	110	26600	17300	1.16
2	P2	Pyrene	84	20600	12200	1.16
3	P3	Pyrene	350	84400	48200	1.28

[a] Polymerization degree as determined by ^{1}H-NMR, [b] Recorded in $CHCl_3$/*i*PrOH/Et_3N 94/2/4 using PMMA standards.

Associated to those three samples, a multi-pyrene PTMPM (**P4**) has been prepared by copolymerizing a mixture of TMPM and pyrene methyl methacrylate (PyrM). A random copolymer structure was targeted to favor the π-π interactions with the CNTs. The PyrM comonomer was prepared from 1-pyrenemethanol using methacryloyl chloride and triethylamine in THF (see Experimental Part). The copolymerization was performed in the same experimental conditions that the ones applied to the homopolymerization while starting with a $[TMPM]_0/[PyrM]_0$ ratio of 5.3 (corresponding to an expected molar ratio of 85/15). Such a ratio has been chosen to favor the π-π interactions between the MWCNTs and the pyrene units along the chains while keeping a high content in redox-active species. After reaction, ^{1}H NMR analysis of the statistical copolymer reveals a [TMPM]/[PyrM] ratio of 82/18 (See Supporting Information, ESI – Entry 1, sample **P4**, Table S1).

Finally, all PTMPM-based (co)polymers were oxidized using an excess of H_2O_2 in the presence of $Na_2WO_4 \cdot 2H_2O$/EDTA. Oxidations were carried out in MeOH at a concentration in (co) polymer of 20 g/L at 50 °C for 24 hours.[4] As expected, the PTMAs-based (co)polymers are showing an orange color consistent with the absorption peak attributed to the nitroxide group around 460 nm. The degree of oxidation determined from the intensity of that peak is 98%. For clarity, each oxidized sample has been named P*n*-ox with *n* corresponding to the number of the sample and going from 1 to 4. Importantly, no degradation of the (co)polymers was observed upon oxidation, as attested by SEC analyses performed on both homo- and copolymers (**P3-P3ox** and **P4-P4ox**, respectively) (ESI, Figure S2).

2.2. Electrochemical Properties

Composites made by blending PTMA-based (co)polymers with MWCNTs were prepared for the generation of electrodes. The composition of the slurry was selected to be 30/60/10 (wt%) in PTMA/CNTs/binder.[25] The elaboration of a slurry showing a good viscosity and favoring the interactions between CNTs and pyrene-based PTMA needed some adjustments of the previously-described procedures/protocols.[26] To favor supramolecular interactions, the two components have to be intimately mixed and NMP was found to be the best solvent to solubilize/disperse PTMA and CNTs. The films obtained via a classical mixing using ball miller were not homogeneous and the associated performances were not satisfactory (data not shown here). To improve the quality of the slurry, CNTs were gradually dispersed in NMP using a sonoprobe, then the PTMA (solubilized in NMP) was added to the dispersion under sonication. The binder was incorporated before further mixing in a ball miller at medium speed (400 rpm) to get a homogeneous slurry. Thin films of this viscous slurry were fabricated/generated by Doctor Blading with a 400 µm thick blade (Bar type Film Applicator). Disks of those composite films were cut, and half-cells were assembled under argon atmosphere in a glove box.

Cyclic voltammetry analyses were performed on these cells to confirm the redox behavior of the PTMA-based (co)polymers (Figure 2). All the (co)polymers display a reversible oxidation

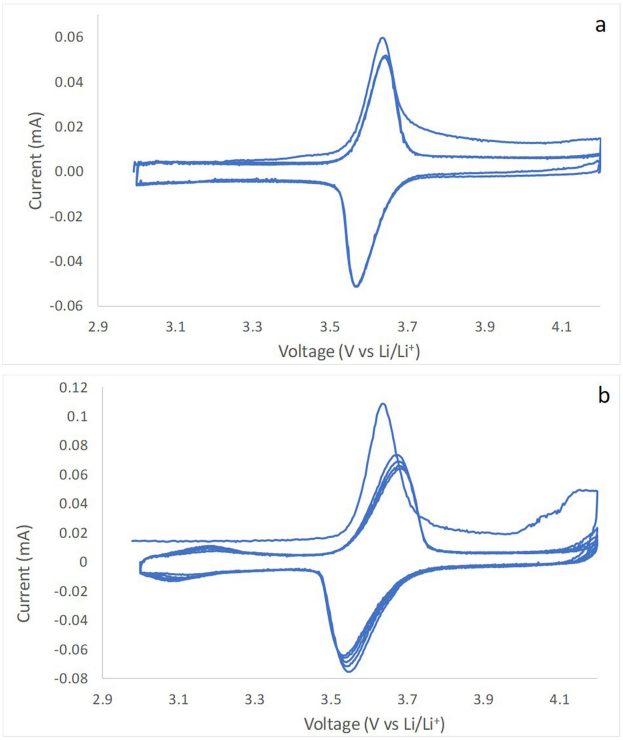

Figure 2. Cyclic voltammograms of PTMA-based (co)polymers. a) Homopolymer **P3ox**. b) Copolymer **P4ox**.

peak centered at 3.6 V vs Li/Li^+, characteristic of the nitroxide radical oxidation into the oxoammonium cation. This process is stable with cycling, with a constant oxidation potential as well as a constant intensity of the oxidation peak as demonstrated by the superimposition of the curves of cycles 2 and 3. The voltammograms of **P3ox** (Figure 2a) and **P4ox** (Figure 2b) exhibit a sharp peak-to-peak separation of 0.09 and 0.14 V vs Li/Li^+, respectively, demonstrating a faster charge transfer for the homopolymer in the electrochemical processes. In the voltammogram of **P4ox**, a second process is visible at lower potential (around 3.1 V vs Li/Li^+). The possible origin of this reversible oxidation peak will be discussed later.

The performances of the PTMA electrodes were recorded during galvanostatic cycles at a current density of C/5 for the three cycles then at C/2 for the following cycles, with a voltage ranging between 3.0 and 4.2 V. The capacity retentions of the (co)polymers over 170 cycles are shown in Figure 3. All the (co)

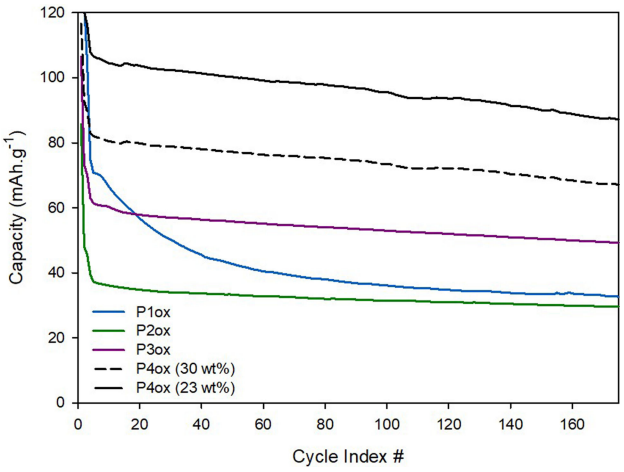

Figure 3. Capacity retention of Pyr-based (co)polymers/CNTs cathodes at C/2 rate over 170 cycles.

polymers show a first drop in the capacity due to irreversible processes. The capacity of **P1ox** shows a continuous, substantial decrease over the first hundred cycles (33% loss). This capacity loss during the charge/discharge cycling is attributed to a partial solubilization of PTMA in the electrolyte, as already observed by others.[10] The pyrene-containing PTMAs shows a much milder decrease over the cycles. The longer monofunctionalized pyrene-based PTMA (**P3ox**) shows a higher initial charge capacity than its shorter counterpart **P2ox** (63 vs 37 mAh g^{-1}). This behavior is probably due to a more pronounced solubilization of the low molar mass polymer in the electrolyte during the equilibration period before the measurements, despite the presence of the anchoring pyrene unit. **P2ox** shows a capacity around 37 mAh g^{-1}, corresponding to 30% of the theoretical capacity. Excluding the first cycles, the capacity stability of this polymer is quite high, around 93% over 170 cycles. **P3ox** shows a capacity around 63 mAh g^{-1} (50% of the theoretical capacity) with a loss of 10% between the 5th and the 170th cycles. The introduction of a single pyrene group on PTMA thus leads to good capacities as soon as the molar mass of the structure is sufficiently high. Moreover, the capacity retention is highly improved with respect to non-functionalized PTMA, even for relatively short pyrene-PTMA chains.

The DFT calculations show that the pyrene molecule adsorbs flat on the graphene surface, interacting with it via π-π interactions. In contrast, the TMA fragment interacts mainly via weaker CH-π interactions; the nitroxide group does not strongly interact with the graphene surface and the radical remains localized on the oxygen atom. Since the adsorption of a single pyrene unit is stronger than that of a TMA by about 3 kcal mol^{-1}, the pyrene functionalization indeed appears as a valuable strategy to improve the anchorage of functionalized PTMA polymer chains on carbon nanotubes.

As expected, the multi-pyrene copolymer **P4ox** presents a well higher initial capacity of above 80 mAh g^{-1} (dashed black line, Figure 3). After 170 cycles, the capacity remains at 70 mAh g^{-1} (67% of the theoretical value). Over this cycling process, the capacity retention is good, with only 13% loss. Those values have been normalized on the basis of a 30 wt% amount of active material in the electrode. On the contrary to both **P2ox** and **P3ox**, the percentage of radical units in the random **P4ox** copolymer is however limited to 77 wt% (82% mol). Considering the real percentage of active redox units (23 wt% instead of 30 wt%), the real capacity value is then larger by 20–25 mAh g^{-1} (full black curve in Figure 3). Note here that such assumption is correct only if the PyrM repeating units present no redox activity. To clarify it, a complementary experiment has been performed by preparing a new copolymer (**P5**, Figure S3) composed by butyl methacrylate (BMA) and PyrM comonomer (no redox unit). BMA was chosen for its non-redox activity. Both comonomers were copolymerized in the same conditions than those used for the preparation of **P4** (ESI, entry 1, Table S1). As expected, no redox activity was observed from an electrode containing **P5**. Galvanostatic cycling led only to very low capacity values of around 10 mAh g^{-1}, which is here attributed to the carbonated material (ESI, Figure S4). The lack of redox activity for PyrM was thus confirmed with this complementary study and attests the capacity calculated for the **P4ox** copolymer.

This last multi-pyrene sample demonstrates high and stable capacities during cycling at C/2, with values well above those of mono-functionalized PTMA (**P2ox** and **P3ox**) or physical blended PTMA (**P1ox**). Performances of this copolymer are also slightly better than the results reported previously for PTMA grafted onto CNTs, which showed a capacity of 80 mAh g^{-1}.[21]

It is important to point out the relatively low molar mass of the **P5ox** copolymer (Mn_{SEC} = 9100 g mol^{-1} vs PMMA standards). Proton NMR did not allow the determination of the real DP; nevertheless, the SEC value is a good indication of the short length of this copolymer (strict comparison is not possible, since the polymer and the copolymer have different hydrodynamic volumes). A pure PTMA with a similar Mn is extremely soluble in the electrolyte and presents low performances during battery testing.

The improved capacity of the multi-pyrene PTMA can originate from two phenomena: on one hand, the pyrene-containing copolymer could be less soluble than the corresponding pure PTMA compound, which would reduce the leaching in the electrolyte. On the other hand, the presence of the pyrene units is likely to induce stronger intermolecular interactions between the polymer chains and the CNT surface, favoring physical anchoring and improving the resistance towards solubilization. To verify such hypothesis, we have modeled the adsorption and compared the adsorption energy on a (77,77) CNT of a chain of the Pyr-PTMA copolymer with that of an equivalent PTMA homopolymer chain. The first step in the modeling is to allow the isolated polymer chain to coil up. The coiled polymer chain is then moved close to the nanotube and its adsorption and equilibration on the CNT are followed during a 10 ns-long MD simulation. We find that both polymer chains adsorb on the nanotube and remain partially coiled (see Figure 4A for Pyr-PTMA). The Pyr-PTMA chain

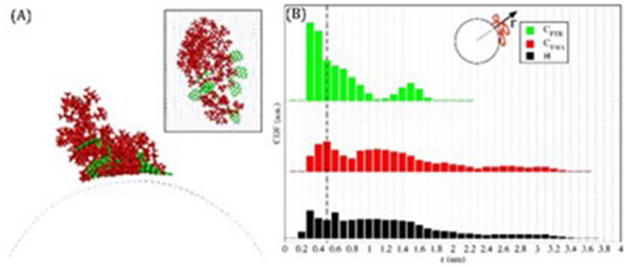

Figure 4. a) Front view of a Pyr-PTMA copolymer chain adsorbed on the (77,77) CNT surface. For the sake of clarity, the CNT was dotted blue and the TMA and Pyr units are colored in red and green, respectively. The inset shows a top view. b) CDFs for the different atomic species considered.

adsorbs in such a way that some of its pyrene groups lie almost flat on the nanotube, promoting π-π interactions. Figure 4B shows the cylindrical distribution functions, CDF, which are a reflection of the distribution of the molecular fragments near the CNT surface, for the carbon atoms in the Pyr and TMA units and for all hydrogen atoms. All the atoms on the left of dashed line placed at 0.5 nm are considered to be in contact with the nanotube wall. Both TMA and pyrene units are present at the surface, but it clearly appears that the density of the latter is much larger than that of the former. Consistently, the segments of the chain that lie far from the nanotube are mostly composed of TMA units, as the corresponding CDF extends up to 3 nm from the surface. These results thus indicate that the pyrene units are preferentially adsorbed on the nanotube.

The adsorption energy, AE, was calculated as the difference between the potential energy of the adsorbed system and the sum of the potential energies for the isolated chain and nanotube (Table 2). The contact surface area between the polymer chain and the nanotube, CSA, was estimated using the 'solvent accessible surface area' method and it is used to calculate the density of adsorption energy, DAE. The DAE allows to readily compare the strength of the polymer-nanotube interactions between the two systems: it is clear that Pyr-PTMA does indeed adsorb much stronger than PTMA on the nanotube.

Table 2. Adsorption Energy, Contact Surface Area, and Density of Adsorption Energy for the Pyr-PTMA and PTMA chains on the CNT.

Polymer on CNT	AE (kJ mol^{-1})	CSA (nm^2)	DAE (kJ mol^{-1} nm^{-2})
Pyr-PTMA	−648.8	10.6	−61.2
PTMA	−565.2	12.0	−47.1

The rate performances of representative **P3ox** and **P4ox** cathodes were studied, increasing the current density from C/15 to 40C and C/11 to 105C, respectively (Figure 5). The charge/discharge capacities are decreasing with increasing the current density, as expected.

At C/7, the **P3ox** cathode delivers 70 mAh g^{-1}. This capacity is decreased by 18% at C, by 40% at 20C and keeps half of the initial value at 40C. The typical plateau of PTMA is centered at 3.6 V vs Li/Li$^+$. At high current density, a spreading of the charge and discharge plateaus is appearing, due to polarization.

At C/6, the **P4ox** cathode delivers a high capacity of 110 mAh g^{-1}. This value is decreased by 25% at C, by 50% at 20C. During charge and discharge, the PTMA plateau is centered around 3.6 V vs Li/Li$^+$. These curves also exhibit a spreading of the plateaus while increasing the current density. This spreading is more pronounced for the discharge, meaning that the polarization is stronger during this part of the redox process. In this case, a second phenomenon is appearing above 4C, with the coexistence of two plateaus that progressively combine. The whole process is visible on the charge and discharge curves at 4C. However, at 9C, even if the charge process seems to display a single plateau at 3.7 V, the discharge process is displaying two distinct redox responses around 3.5 V and 3.4 V.

Upon increasing the cycling rate up to 52C, this discharge behavior is still present but tends to disappear as the redox responses begin to merge in a single one with $E_{1/2}$ around 3.6 V. Considering the reversibility for each cycling rate, it seems reasonable that for all discharge curves obtained between 4C and 52C, the different faradic responses should still be related to the PTMA redox process only. This discharge behavior can be related to an inhomogeneity of the cathode, with areas showing different performances depending of the current density. This could originate from a partial ion diffusion issue. At low current density, a slope change is clearly visible around 3.2 V vs Li/Li$^+$. This process cannot be attributed to PTMA since no mirror effect centered at 3.6 V vs Li/Li$^+$ is observed in the charge curve. This inflexion that is clearly visible at low current density disappears at higher value, confirming the process dependency on the current density. According to the literature, this value is neither related to traces of the amine precursor of the nitroxide function, nor to CNTs. This slope change could hardly be related to traces of residual catalyst (from the CNTs synthesis or from the polymer synthesis) since metallic catalysts are oxidized below 3 V vs Li/Li$^+$. Another possible origin could be a redox activity of the pyrene unit. This hypothesis was considered but no proof could be found on the voltammogram

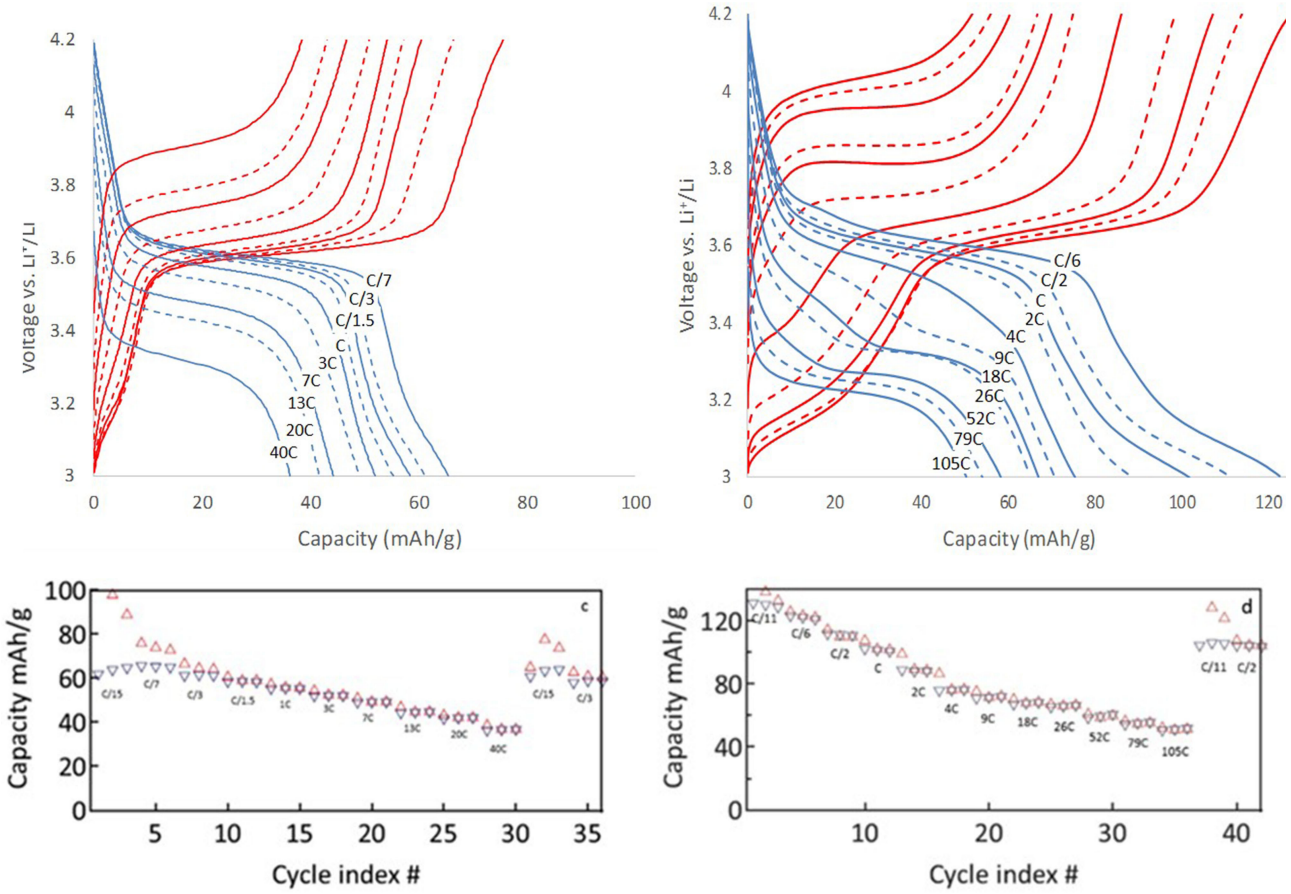

Figure 5. Charge/discharge curves and rate performances of P3ox/CNTs (a, c) and P4ox/CNTs (b, d) cathodes under variable C rates.

of **P5**. Still another possibility explaining this inflexion could be traces of oxidation residues (EDTA, Na_2WO_4), which would contaminate the samples despite the purification steps.

Finally, the systems were cycled back to low C rates showing values similar to the initial capacities, thus demonstrating a good stability of the cathodes.

3. Conclusions

In this work, we synthesized pyrene-based poly(2,2,6,6-tetramethylpiperidinyloxy-4-yl methacrylate) with one pyrene end-group and bearing multiple pyrene units along the polymer backbone, to study the effect of the pyrene number. Copolymerization was achieved using ATRP to access a defined molecular weight and pyrene/TMA ratio. These copolymers were blended with carbon nanotubes to prepare cathodes for batteries. Composite materials of copolymer/CNTs/binder were prepared with a 30/60/10 ratio and incorporated in half-cells. Electrochemical behavior of the cells attested an improvement of the capacity as well as the cycling stability due to the introduction of pyrene in the PTMA. This effect is even enhanced for the copolymer containing 18 mol% of pyrene with capacities reaching 105 mAh g^{-1} at a C/2 rate and a loss of 13% over 180 charge/discharge cycles. Its performance under variable C rates confirm the good stability of the cathodes with still a capacity of 50 mA g^{-1} at 105C. The interaction of the pyrene units with the CNTs was confirmed through quantum-chemical and molecular modeling simulations, showing a stronger adsorption of the pyrene-based PTMA on CNTs compared to PTMA.

Experimental Section

Materials

Toluene (VWR, 99%), tetrahydrofuran (THF, VWR, 99%) and dichloromethane (CH_2Cl_2, VWR, 99%) were dried using an MBraun solvent purification system under N_2. Multiwall carbon nanotubes NC7000 (MWCNT) were provided by Nanocyl. 1-Pyrenemethanol (98%, Aldrich), bromoisobutyryl bromide (98%, Aldrich), 2,2,6,6-tetramethyl-4-piperidyl methacrylate (TMPM, >98%, TCI), copper(I) bromide (CuBr, 98%, Sigma Aldrich), 1,1,4,7,10,10-hexamethyltriethylenetetramine (HMTETA, 97%, Aldrich), sodium tungstate dihydrate ($Na_2WO_4 \cdot 2H_2O$, ≥99%, Sigma Aldrich), hydrogen peroxide solution (50% vol, VWR), ethylenediaminetetraacetic acid disodium salt dihydrate (EDTA, ≥98%, Sigma Aldrich), methacryloyl chloride (97%, Aldrich), triethylamine (≥99% Merck), and all other chemicals were used as received.

Synthetic Procedures

Pyrene Methyl-α-Bromoisobutyrate (Pyr-Ini)

In a two-necked round-bottom flask, 1-pyrene methanol (2 g, 8.6 mmol, 1 eq.) is solubilized into 50 mL of a toluene/THF (4/1) mixture. Bromoisobutyryl bromide (1.2 mL, 9.7 mmol, 1.13 eq.), previously solubilized in 5 mL of THF, is added dropwise to the alcohol solution at 0 °C. The mixture is stirred overnight at r.t. After filtration, the residue is washed with water (3x) and dried under vacuum (3.16 g, $\eta = 96\%$). ^{1}H NMR (500 MHz, $CDCl_3$) δ (ppm): 1.94 (6H, s), 5.92 (2H, s), 8.02–8.30 (9H, m)

Pyrene Methyl Methacrylate (Pyr-M)

In a two-necked round-bottom flask, 1-pyrene methanol (1 g, 4.3 mmol, 1 eq.) is solubilized into 50 mL of dry THF. Et_3N (1.25 mL, 12.9 mmol, 3 eq.) is added and the mixture is cooled down to 0 °C. Methacryloyl chloride (1.8 mL, 12.9 mmol, 3 eq.) is added dropwise under N_2 and the medium is allowed to warm up to r.t. and kept under stirring for 12 hours. After filtration of the NEt_3.HCl salt, the solvent is removed. The residue is solubilized in Et_2O and washed twice with water. The organic layer is dried over $MgSO_4$, filtered and concentrated. The purification was done by recrystallization in EtOH (50 ml) at 40 °C, filtrated while hot and the solid was dried under vacuum. Pyr-M was obtained as a white solid (480 mg, $\eta =$ 37%). ^{1}H NMR (500 MHz, $CDCl_3$) δ(ppm): 1.98 (3H, s), 5.57 (1H, s), 5.92 (2H, s), 6.16 (1H, s), 8.02–8.33 (9H, m)

Typical Procedure for the Synthesis of Pyr-PTMPM (P2, P3)

In a round-bottom flask, a solution of Pyr-Ini (20 mg, $5.3 \cdot 10^{-5}$ mol, 1 eq.), TMPM (3 g, 13 mmol, 250 eq.) and HMTETA (30 μL, 0.11 mmol, 2 eq.) in 4.2 mL of anhydrous THF was degassed by 3 freeze-pump-thaw cyclings. In a second round-bottom flask, CuBr (8 mg, $5.3 \cdot 10^{-5}$ mol, 1 eq.) was degassed by vacuum-nitrogen cycles. After the transfer of the monomer mixture onto CuBr, the resulting solution was degassed one more time by a freeze-pump-thaw cycle then heated at 90 °C for 2 hours. The polymerization was quenched by cooling down the reaction and putting it back to air. After filtration on basic alumina with DCM, the solvent was removed. The residue was solubilized in a small amount of DCM and precipitated in cold pentane. The white solid was isolated by filtration and dried at 40 °C under vacuum (1.962 g, $\eta = 47\%$).

Typical Procedure for the Synthesis of P(TMPM-r-PyrM) (P4)

In a round-bottom flask, a solution of Pyr-Ini (21 mg, $5.5 \cdot 10^{-5}$ mol, 1 eq.), TMPM (1 g, 4.4 mmol, 80 eq.), Pyr-M (250 mg, 0.83 mmol, 15 eq.) and HMTETA (30 μL, 0.11 mmol, 2 eq.) in 3 mL of anhydrous THF was degassed by 3 freeze-pump-thaw cyclings. In a second round-bottom flask, CuBr (8 mg, $5.5 \cdot 10^{-5}$ mol, 1 eq.) was degassed by vacuum-nitrogen cycles. After the transfer of the monomer mixture onto CuBr, the resulting solution was degassed one more time by a freeze-pump-thaw cycle then heated at 90 °C for 2 hours. The polymerization was quenched by cooling down the reaction and putting it back to air. After filtration on basic alumina with DCM, the solvent was removed. The residue was solubilized in a small amount of DCM and precipitated in cold pentane. The white solid was isolated by filtration and dried at 40 °C under vacuum (350 mg, $\eta = 33\%$).

Typical Procedure for the Oxidation of PTMPM-Based (Co) Polymers into PTMA (Co)Polymers (Pox): In a round-bottom flask Pyr-PTMPM (1.5 g, 6.5 mmol), $Na_2WO_4 \cdot 2H_2O$ (600 mg, 1.8 mmol, 0.28 eq. vs N–H) and EDTA.2Na (390 mg, 1 mmol, 0.16 eq. vs N–H) are solubilized in 70 mL of MeOH. The mixture is heated at 60 °C for 10 to 15 min, then H_2O_2 (7.5 mL, 0.13 mol, 20 eq. vs N–H) is added slowly and the reaction is carried out at the same temperature for 24 hours. At r.t., the mixture is extracted with DCM, the organic layer is washed with water (3 times) and dried over $MgSO_4$. After filtration, the solvent is removed and a purification is realized by re-precipitation in pentane to obtain the oxidized polymer as an orange solid (1.331 g, $\eta = 83\%$).

Electrochemical Characterizations

Slurry Preparation

The composition of the polymer/CNTs/kynarflex slurry was selected to be 30/60/10 (wt%) because it showed the best specific capacities for PTMA-based electrodes.[25]

CNTs (100 mg) were dispersed in NMP (3 g) in three fractions using 10 seconds of sonoprobe sonication in between each addition. Then the polymer (50 mg) solubilized in NMP (1 g) was introduced in three fractions staggered by a sonication pulse of 10 s. Finally, the binder (Kynar Flex) was added (16.7 mg) to the mixture.

Electrode Preparation

The slurry was mixed using a ball miller for 30 minutes. The viscous mixture was deposited onto an aluminum carbon coated foil using a Doctor Blade. The films were then dried at 70 °C on a hot plate, then stored in a vacuum oven at 70 °C for few days. The films were cut into disks (0.5 inch (~12.5 mm) diameter) for electrochemical measurements.

Cell Assembly

Cathodes were tested in half-cell configuration. Coin cells were assembled in a glovebox under an argon atmosphere (< 0.1 ppm H_2O, < 0.1 ppm O_2). CR2032 spare parts coin cells were purchased from MTI Corp. The electrolyte was a mixture of ethylene carbonate (EC) and diethylcarbonate (DEC) in a ratio 1:1 (v:v) with 1 M of lithium hexafluorophosphate ($LiPF_6$) from Solvionic. The separator was a porous polyethylene membrane purchased from Celgard. Lithium metal foils purchased from Gelon were used as reference and counter electrode.

Electrochemical Measurements: Cyclic voltammetry and charge/discharge cycles were recorded on an Arbin Instrument Battery Tester BT-2043.

Modeling Methodology: To gain a better understanding of the quality of the interactions between the pyrene-PTMA polymer chains and the carbon nanotubes, we performed quantum-chemical DFT calculations on isolated pyrene and TMA fragments interacting with a graphene flake. The graphene flake is used as a model for the external wall of the nanotube and the physisorption of the molecular fragment has been assessed with Eq. 1. The uwB97xd DFT functional was used with the 6-31g** basis set; the counterpoise method was used to estimate the Basis Set Superposition Error (BSSE).

$$AE = E_{sys} - (E_{mol} + E_{gr}) - BSSE \quad (1)$$

Where AE is the adsorption energy, E_{sys} the total energy of the system, E_{mol} and E_{gr} the potential energies of the molecular

fragment and the graphene flake as isolated, non-interacting, species.

To study the physisorption of the polymer chains on carbon nanotubes, we built a 60 monomer-long, random Pyr-PTMA copolymer chain having a molecular mass of 15000 and a 15:85 Pyr:TMA composition, which is representative of the real copolymers. This polymer is made to interact with a (77,77) single-wall nanotube with a diameter of about 10 nm. These calculations have been carried out by means of Molecular Dynamics (MD) simulations in vacuum at 300 K. The MD simulations were performed with the Gromacs 2016 molecular code and the Amber99sb force field. The Nose-Hoover thermostat was used to control the temperature and the LINCS algorithm was used to constrain the bond length to the force field value. The nanotube was considered as a periodic rigid body representing the outer surface of a typical MWCNT. Cylindrical Distribution Functions (CDF), which are a statistical measure of the positions of the different atoms with respect to the nanotube wall, were collected over the last 5 ns of the MD simulations, once the polymer chains have equilibrated.

Acknowledgements

The authors are grateful to the HYB2HYB and BATWAL projects from the DGO6 of the Service Public de Wallonie. Computational resources have been provided by the Consortium des Equipements de Calcul Intensif (CECI), funded by the Fonds de la Recherche Scientifique (F.R.S.-FNRS) under Grant No. 2.5020.11. O.C is FRS-FNRS Research Associate.

Conflict of Interest

The authors declare no conflict of interest.

Keywords: batteries · density functional calculations · nanotubes · polymers · pyrene

[1] Y. Tang, Y. Zhang, W. Li, B. Ma, X. Chen, *Chem. Soc. Rev.* **2015**, *44*, 5926.
[2] A. S. Arico, P. Bruce, B. Scrosati, J.-M. Tarascon, W. van Schalkwijk, *Nat. Mater.* **2005**, *4*, 366.
[3] T. Janoschka, M. D. Hager, U. S. Schubert, *Adv. Mater.* **2012**, *24*, 6397.
[4] J.-K. Kim, G. Cheruvally, J.-W. Choi, J.-H. Ahn, S. H. Lee, D. S. Choi, C. E. Song, *Solid State Ionics* **2007**, *178*, 1546.
[5] Y. Liang, Z. Tao, J. Chen, *Adv. Eng. Mater.* **2012**, *2*, 742.
[6] W. Huang, *Polymer science: research advances, practical applications and educational aspects (A. Mendez-Vilas; A. Solano, Eds.)* **2016**.
[7] T. Suga, Y.-J. Pu, K. Oyaizu, H. Nishide, *Bull. Chem. Soc. Jpn.* **2004**, *77*, 2203; K.-A. Hansen, P. James, *Polym. Chem.* **2018**, *9*, 1479.
[8] H. Nishide, S. Iwasa, Y.-J. Pu, T. Suga, K. Nakahara, M. Satoh, *Electrochim. Acta* **2004**, *50*, 827.
[9] L. Cao, S. Sadaf, S. M. Beladi-Mousavi, L. Walder, *Eur. Polym. J.* **2013**, *49*, 1923.
[10] W. Guo, Y.-X. Yin, S. Xin, Y.-G. Guo, L.-J. Wan, *Energy Environ. Sci.* **2012**, *5*, 5221.
[11] K. Zhang, Y. Hu, L. Wang, J. Fan, M. J. Monteiro, Z. Jia, *Polym. Chem.* **2017**, *8*, 1815.
[12] F. Boujioui, O. Bertrand, B. Ernould, J. Brassinne, T. Janoschka, U. S. Schubert, A. Vlad, J.-F. Gohy, *Polym. Chem.* **2016**, *8*, 441.
[13] L. Bugnon, C. J. H. Morton, P. Novak, J. Vetter, P. Nesvadba, *Chem. Mater.* **2007**, *19*, 2910.
[14] G. Hauffman, A. Vlad, T. Janoschka, U. S. Schubert, J. F. Gohy, *J. Mater. Chem. A* **2015**, *3*, 19575.
[15] S. Iwasa, T. Nishi, H. Sato, S. Nakamura, *J. Electrochem. Soc.* **2017**, *164*, A884.
[16] M.-K. Hung, Y.-H. Wang, C.-H. Lin, H.-C. Lin, J.-T. Lee, *J. Mater. Chem.* **2012**, *22*, 1570.
[17] Y. Li, Z. Jian, M. Lang, C. Zhang, X. Huang, *ACS Appl. Mater. Interfaces* **2016**, *8*, 17352.
[18] R. Peng, Y. Wang, W. Tang, Y. Yang, X. Xie, *Polymer* **2013**, *5*, 847.
[19] K. Zhang, Y. Hu, L. Wang, M. J. Monteiro, Z. Jia, *ACS Appl. Mater. Interfaces* **2017**, *9*, 34900.
[20] B. Ernould, M. Devos, J.-P. Bourgeois, J. Rolland, A. Vlad, J.-F. Gohy, *J. Mater. Chem. A* **2015**, *3*, 8832.
[21] B. Ernould, O. Bertrand, A. Minoia, R. Lazzaroni, A. Vlad, J.-F. Gohy, *RSC Adv.* **2017**, *7*, 17301.
[22] S. Bose, A. R. Bhattacharyya, A. R. Kulkarni, P. Pötschke, *Compos. Sci. Technol.* **2009**, *69*, 365.
[23] N. Karousis, N. Tagmatarchis, D. Tasis, *Chem. Rev.* **2010**, *110*, 5366.
[24] G. Hauffman, J. Rolland, J.-P. Bourgeois, A. Vlad, J.-F. Gohy, *J. Polym. Sci. Part A: Polym. Chem.* **2013**, *51*, 101.
[25] J.-K. Kim, G. Cheruvally, J.-H. Ahn, Y.-G. Seo, D. S. Choi, S.-H. Lee, C. E. Song, *J. Ind. Eng. Chem.* **2008**, *14*, 371.
[26] K. Nakahara, J. Iriyama, S. Iwasa, M. Suguro, M. Satoh, E. J. Cairns, *J. Power Sources* **2007**, *165*, 870.

Manuscript received: April 16, 2018
Version of record online: June 25, 2018